
Adaptive Heterogeneous Mixtures of Normalising Flows for Robust Variational Inference

Benjamin Wiriaypong

Oktay Karakus

Kirill Sidorov

School of Computer Science and Informatics, Cardiff University, CF24 4AG, UK.

{wiriaypong, karakuso, sidorovk}@cardiff.ac.uk

Abstract

Normalising-flow variational inference (VI) can approximate complex posteriors, yet single-flow models often behave inconsistently across qualitatively different distributions. We propose *Adaptive Mixture Flow Variational Inference* (AMF-VI), a heterogeneous mixture of complementary flows (MAF, Re-ALNVP, RBIG) trained in two stages: (i) sequential expert training of individual flows, and (ii) adaptive *global* weight estimation via likelihood-driven updates, without per-sample gating or architectural changes. Evaluated on six canonical posterior families of *banana*, *X-shape*, *two-moons*, *rings*, *a bimodal*, and *a five-mode mixture*, AMF-VI achieves consistently lower negative log-likelihood than each single-flow baseline and delivers stable gains in transport metrics (Wasserstein-2) and maximum mean discrepancy (MDD), indicating improved robustness across shapes and modalities. The procedure is *efficient and architecture-agnostic*, incurring minimal overhead relative to standard flow training, and demonstrates that adaptive mixtures of diverse flows provide a reliable route to robust VI across diverse posterior families whilst preserving each expert’s inductive bias.

1 Introduction

Variational inference (VI) is widely used for approximate Bayesian computation, yet complex *multimodal* posteriors remain challenging. Classical VI with simple families (e.g., Gaussians) lacks the capacity to represent multiple modes, leading to underestimated uncertainty and poor fits (Bishop and Nasrabadi, 2006). Normalising flows increase expressiveness (Kobyzev et al., 2020; Papamakarios et al., 2021), but individual architectures often specialise to particular structures and can suffer mode collapse during optimisation (Che et al., 2016), limiting reliability in applications such as generative modelling, Bayesian neural networks, and hierarchical posteriors.

Multimodality is a *practical* requirement in many domains: hierarchical Bayesian models can yield distinct epidemiological regimes (Wakefield, 2007), deep generative models often induce discrete semantic clusters (Kingma and Welling, 2013), and financial returns switch across market regimes (Ang and Bekaert, 2002; Hamilton, 1989). While normalising flows have shown strong capacity to model such structure (Kobyzev et al., 2020; Papamakarios et al., 2021), single-flow architectures face a bias–variance tension when asked to cover diverse modes with one parametric family. This motivates mixture-based flows that can *adaptively* allocate capacity across modes while remaining computationally tractable for variational inference (Blei et al., 2017a).

Current mixture-enhanced flows typically use *global*, *data-independent* mixing weights $\{\pi_k\}$ learned once and fixed at test time (Pires and Figueiredo, 2020; Ng and Zammit-Mangion, 2024; Izmailov et al., 2019; Kobyzev et al., 2021; Bishop, 2006; Dempster et al., 1977). Such global weighting struggles to reallocate mass to local complexities (secondary modes, tails), a problem exacerbated under the *reverse* divergence $\text{KL}(q\|p)$, which is mode-seeking and can under-disperse (Blei et al., 2017b). Although tail-aware VI objectives (Wang et al., 2018) and base-distribution tweaks (Stimper et al., 2022) help, a gap remains between the *adaptive* nature of targets and the *global* structure of many mixture-of-flows designs, where tractable *dynamic* allocation across the full support is still challenging (Kobyzev et al., 2021). Related experience with mixture density networks reports instability and mode under-representation without extra mechanisms (Bishop, 2006; Makansi et al., 2019), underscoring the need for mixtures that *adapt allocation* rather than fixing it globally.

Despite substantial progress in normalising-flow architectures—e.g., RealNVP (Dinh et al., 2016), Masked Autoregressive Flow (MAF) (Papamakarios et al., 2017), and Rotation-based Iterative Gaussianisation (RBIG) (Laparra et al., 2011)—there remains a need for a principled, tractable way to *combine* heterogeneous flows for reliable multimodal posterior inference across diverse geometries. Individual flows offer complementary strengths (RealNVP’s efficient coupling layers for high-dimensional transforms, MAF’s strong density estimation, RBIG’s robust iterative Gaussianisation), suggesting that adaptive component selection could improve approximation quality (Rezende and Mohamed, 2015; Chen et al., 2018). However, existing mixture approaches in VI often use fixed global weights or heuristic adaptation, which under-exploit the interplay between component specialisation and target structure (Tomczak and Welling, 2018; Berg et al., 2018). Moreover, current work on mixture normalising flows has not fully addressed learning data-driven *optimal* combinations, nor explored sequential training strategies that leverage meta-learning to improve coordination and convergence (Finn et al., 2017; Nichol et al., 2018).

The absence of sophisticated frameworks for adaptive sampling from learned mixture components represents a critical gap in the current literature, particularly given the potential for dynamically adjusting component importance based on local distribution complexity and sampling requirements (Loaiza-Ganem and Cunningham, 2019; Behrmann et al., 2019). Existing approaches to mixture model adaptation in related domains, such as mixture of expert architectures (Shazeer et al., 2017) and ensemble methods (Lakshminarayanan et al., 2017), have not been systematically adapted to the unique challenges posed by normalising flow mixtures, where maintaining invertability and tractable density computational challenges. Additionally, the lack of comprehensive analysis regarding how different flow architectures specialise within mixture context, including their respective abilities to capture specific modes, handle varying local curvatures, and maintain stable training dynamics, represents a significant obstacle to developing principled mixture design strategies which could substantially advance the state of variational inference for complex, multimodal distributions.

Motivation and aims. This work develops an *adaptive mixture* framework for normalising flows that tackles a core limitation of single-flow architectures: brittle behaviour across qualitatively different posterior geometries. Our objective is to combine heterogeneous inductive biases through *data-driven global weighting* while keeping the training pipeline lightweight and reproducible. Concretely, we investigate (i) *sequential* training protocols

in which individual flows specialise on complementary aspects of the target before combination, connecting to multi-stage learning and curriculum ideas (Bengio et al., 2009) and ensemble methodology (Breiman, 2001); (ii) *non-parametric* weight adaptation based on likelihood-driven moving-average updates that adjust component importance without per-sample gating, informed by mixture-of-experts principles (Jacobs et al., 1991) and adaptive learning frameworks (Sutton et al., 1998); and (iii) rigorous evaluation beyond log-likelihood, incorporating distributional distance and transport-theoretic metrics (Villani, 2008). The goal is a practical, architecture-agnostic recipe that yields robust posterior approximation across diverse families while retaining the simplicity of standard flow training.

Contributions. We introduce *Adaptive Mixture Flow Variational Inference* (AMF-VI), a heterogeneous mixture of normalising flows (MAF, RealNVP, RBIG) trained in two stages: *Stage 1* trains experts *sequentially* and independently; *Stage 2* estimates *global* mixture weights post hoc via likelihood-driven moving-average updates (softmax-normalised), with a light smoothing/floor to avoid degenerate collapse. No per-sample gating or end-to-end joint training is required. We evaluate on six canonical posterior families, *banana*, *X-shape*, *two-moons*, *rings*, *a bimodal*, and *a five-mode mixture* and report five complementary metrics: negative log-likelihood (NLL), Kullback–Leibler (KL) divergence, Wasserstein-2 (W_2) distance, and maximum mean discrepancy (MDD) in unbiased and biased forms. Empirically, AMF-VI achieves consistently lower NLL than each single-flow baseline across these families and exhibits stable improvements in W_2 /MDD, indicating enhanced robustness to shape and modality variation under a minimal training and implementation footprint.

The rest of the paper is organised as follows: Section 2 formulates AMF-VI, where Section 3 presents dataset details and evaluation metrics. Section 4 presents quantitative and qualitative results with ablations. Section 5 discusses limitations and computational trade-offs and concludes the paper.

2 Methodology

This section presents AMF-VI, a two-stage, heterogeneous mixture of normalising flows for posterior approximation. In **Stage 1**, architecturally diverse experts (e.g., MAF, REALNVP, RBIG) are trained *independently*, where in **Stage 2**, with expert parameters fixed, we estimate *global* mixture weights by a likelihood-driven moving-average update, yielding a tractable, data-agnostic gate that reallocates mass across experts without per-sample gating. The remainder of this section formalises the mixture, details weight learning, motivates the moving-average scheme, and summarises the expert classes.

2.1 Mixture Model Formulation

2.1.1 Mixture Posterior Approximation

The central construct in AMF-VI is the mixture posterior approximation, defined as:

$$q_\phi(z) = \sum_{k=1}^K \pi_k q_k(z|\phi_k) \quad (1)$$

where $z \in \mathbb{R}^d$ represents the latent variables, K denotes the number of mixture components, π_k are the mixing weights satisfying $\sum_{k=1}^K \pi_k = 1$ and $\pi_k \geq 0$ for all k , and $q_k(z|\phi_k)$ represent the k -th component density parameterised by ϕ_k (Rezende and Mohamed, 2015; Kingma and Welling, 2013).

Each component $q_k(z|\phi_k)$ is typically implemented as a normalising flow, enabling the transformation of a simple base distribution (usually standard Gaussian) into a more complex, expressive distribution through a sequence of invertible mapping (Papamakarios et al., 2021). This formulation allows the mixture to capture multi-modal posterior distributions that single-component variational approximations often fail to represent adequately.

2.1.2 Role of Mixing Weights and Component parameters

The mixing weights π_k serve a dual purpose in the AMF-VI framework. First, they determine the relative importance of each component in the mixture, effectively controlling the probability mass allocated to different regions of the latent space (Bishop and Nasrabadi, 2006). Second, in the adaptive setting, these weights can be

dynamically adjusted during training to focus computational resources on the most relevant components, leading to improved efficiency and convergence properties (Tomczak and Welling, 2018).

2.2 Learning the Mixing Weights

Mixture models typically learn component weights alongside component parameters through joint optimisation. However, when combining flows with heterogeneous architectures, such as parametric autoregressive models and non-parametric iterative transformations, joint training requires careful balancing of learning rates and convergence criteria across fundamentally different optimisation procedures. Our sequential AMF-VI framework addresses this practical challenge through a two-stage training methodology: first, each flow expert specialises independently; second, mixture weights adapt through a moving average of component performances. This decoupling achieves robust specialisation without the complexity of coordinating heterogeneous optimisation procedures.

2.2.1 Sequential Training Architecture

Our Sequential AMF-VI framework employs a two-stage training methodology that differs from traditional responsibility-weighted approaches. Our method uses sequential training to achieve flow specialisation through temporal separation and performance-based weight adaptation.

The mixture weights π_k are constrained to the probability simplex, satisfying $\sum_{k=1}^K \pi_k = 1$ and $\pi_k \geq 0$ for all k . Rather than parameterising these weights through unconstrained logits and applying softmax transformations, our approach directly updates the weights in the probability simplex through performance-weighted moving averages. This direct parameterisation maintains numerical stability and ensures automatic normalisation throughout the training process.

The key departure from traditional mixture training lies in the temporal separation of flow parameter optimisation and weight training. This approach prevents the instability that can arise from simultaneous optimisation of both flow parameters and mixture weights, particularly when dealing with heterogeneous flow architectures with vastly different convergence characteristics (Bishop and Nasrabadi, 2006).

2.2.2 Two-Stage Training Dynamics

Our training procedure consists of two distinct phases that enable effective specialisation without the computational overhead of full responsibility-weighted training:

Stage 1: Independent Flow Specialisation: Each flow expert q_k is trained independently to maximise its individual log-likelihood:

$$\theta_k^* = \arg \max_{\theta_k} \mathbb{E}_{z \sim q_k} [\log q_k(z | \theta_k)] \quad (2)$$

The implementation accommodates both parametric flows (MAF, RealNVP) through standard gradient-based optimisation and non-parametric flow (RBIG) through specialised fitting procedures. This stage establishes diverse initial representations by allowing each flow to develop its optimal parameters independently, ensuring that different architectural biases lead to complementary specialisations.

Stage 2: Performance-Weighted Moving Average Adaptation: With flow parameters fixed at θ_k^* , the mixture weights are updated directly in the probability simplex using an exponential moving average of normalised flow performances:

$$\pi_k^{(t+1)} = \beta \pi_k^{(t)} + (1 - \beta) \cdot \frac{\exp(\ell_k^{(t)})}{\sum_{j=1}^K \exp(\ell_j^{(t)})} \quad (3)$$

where $\ell_k^{(t)} = \mathbb{E}_{z \sim p_{\text{fresh}}} [\log q_k(z | \theta_k^*)]$ represents the average log-likelihood of the k -th flow on freshly sampled data, and $\beta = 0.9$ is the momentum parameter. The softmax normalisation of log-likelihoods $\exp(\ell_k^{(t)}) / \sum_j \exp(\ell_j^{(t)})$ produces performance-based target weights that favour flows with higher likelihoods, whilst the moving average provides temporal smoothing to prevent rapid weight oscillations. This update rule maintains $\sum_k \pi_k^{(t+1)} = 1$ automatically through the convex combination of normalised distributions.

2.3 Advantages of Moving Average Weight Adaptation

The moving average weight adaptation mechanism provides several critical advantages over traditional gradient-based optimisation approaches:

1. *Computational Efficiency*: The absence of gradient computation and back-propagation through mixture weights significantly reduces training time and memory requirement compared to joint optimisation schemes
2. *Numerical Stability*: The exponential smoothing formulation eliminates gradient explorations or vanishing gradients in weight learning, preventing rapid oscillations that can destabilise mixture training, particularly when combining flows with disparate numerical characteristics
3. *Interpretability*: Mixture weights directly reflect individual flow performance, enabling transparent understanding of component contributions to the overall approximation
4. *Fresh Data Evaluation*: Using a newly generated sampler for weight updates prevents overfitting to specific training batches and provides unbiased performance estimates of each flow's generation capability
5. *Trade-off with Convergence Guarantees*: Unlike joint EM optimisation, this approach does not guarantee convergence to the same local optima. However, the sequential nature avoids the practical challenges of balancing learning rates between heterogeneous flow architectures, which often require extensive hyper-parameter tuning in joint training (McLachlan and Krishnan, 2008).

These advantages make the moving average approach particularly suitable for heterogeneous mixture models where flows have disparate convergence behaviours and architectural properties. The effectiveness of this framework depends critically on the diversity of the component flows, which we detail in the following section.

2.4 Heterogeneous Flow Experts

Our framework combines three architecturally distinct normalising flows, each bringing complementary inductive biases:

Masked Autoregressive Flow (MAF) (Papamakarios et al., 2017) models dependencies through autoregressive transformations:

$$z_i = \mu_i(\mathbf{z}_{<i}; \theta) + \sigma_i(\mathbf{z}_{<i}; \theta) \odot \epsilon_i \quad (4)$$

where $\mathbf{z}_{<i} = (z_1, \dots, z_{i-1})$ denotes previous dimensions and $\epsilon_i \sim \mathcal{N}(0, 1)$.

RealNVP (Dinh et al., 2016) employs affine coupling layers:

$$\mathbf{z}_{1:d} = \mathbf{z}_{1:d} \quad (5)$$

$$\mathbf{z}_{d+1:D} = \mathbf{z}_{d+1:D} \odot \exp(s(\mathbf{z}_{1:d}; \theta)) + t(\mathbf{z}_{1:d}; \theta) \quad (6)$$

where $s(\cdot)$ and $t(\cdot)$ are scale and translation networks.

RBIG (Laparra et al., 2011) alternates rotation and marginal Gaussianisation:

$$\mathbf{z}^{(l+1)} = R^{(l)} \circ G^{(l)}(\mathbf{z}^{(l)}) \quad (7)$$

where $G^{(l)}$ applies marginal Gaussianisation and $R^{(l)}$ is an orthogonal rotation.

The three flows provide complementary modelling capabilities through their distinct architectural constraints. MAF's autoregressive structure enforces explicit sequential dependencies between dimensions, RealNVP's coupling layers enable efficient parallel computation through dimension partitioning, and RBIG's non-parametric approach adapts to arbitrary marginal distributions without parametric assumptions.

The sequential training framework allows each flow to converge independently before weight adaptation begins, avoiding the practical challenges of balancing learning rates across architectures with different optimisation characteristics. The moving average weight updates, then allocate mixture responsibility based on empirical performance, creating an ensemble that leverages the strengths of different architectural priors.

2.5 Adaptive Mixture Flow Variational Inference (AMF-VI)

AMF-VI is a two-stage heterogeneous mixture of normalising flows. In **Stage 1**, experts (MAF, REALNVP, RBIG) are trained *independently* to specialise; in **Stage 2**, with expert parameters frozen, *global* mixture weights

Algorithm 1 AMF-VI: two-stage training with global weights

Require: Experts $\{q_k(z | \theta_k)\}_{k=1}^K$, generator p_{data} , momentum $\beta \in [0, 1)$, epochs T

Stage 1: expert specialisation (independent training)

- 1: **for** $k \leftarrow 1 \dots K$ **do**
- 2: **while** not converged **do**
- 3: Sample batch $z \sim p_{\text{data}}$
- 4: $\theta_k \leftarrow \theta_k + \eta \nabla_{\theta_k} \log q_k(z | \theta_k)$ ▷ RBIG uses its own fitting
- 5: **end while**
- 6: Freeze $\theta_k^* \leftarrow \theta_k$
- 7: **end for**
- 8: Initialise $\pi^{(0)} \leftarrow \text{Uniform}(K)$

Stage 2: global weight adaptation (moving average on simplex)

- 9: **for** $t \leftarrow 0 \dots T-1$ **do**
- 10: Sample fresh batch $z \sim p_{\text{fresh}}$
- 11: **for** $k \leftarrow 1 \dots K$ **do**
- 12: $\ell_k^{(t)} \leftarrow \frac{1}{B} \sum_z \log q_k(z | \theta_k^*)$ ▷ average log-likelihood
- 13: **end for**
- 14: $w \leftarrow \text{softmax}(\ell^{(t)})$
- 15: $\pi^{(t+1)} \leftarrow \beta \pi^{(t)} + (1-\beta) w$ ▷ EMA; stays on simplex
- 16: **end for**
- 17: **return** $q(z) = \sum_k \pi_k^{(T)} q_k(z | \theta_k^*)$ ▷ $N_{\text{eff}} = \exp(H(\pi^{(T)}))$

π are updated by a likelihood-driven moving average on fresh data. Algorithm 1 summarise the procedure; the following paragraphs provide details.

The core innovation lies in the two-stage training dynamics, wherein each flow expert-MAF, RealNVP, and RBIG-first undergoes independent optimisation to develop distinct representational capacities. MAF excels at capturing autoregressive dependencies through its sequential structure, RealNVP provides computational efficiency via coupling layer transformations, whilst RBIG offers non-parametric robustness for heavy-tailed and outlier-prone distributions. Following this specialisation phase, the framework employs a moving average weight adaptation mechanism that uses fresh data evaluation to prevent overfitting and ensure generalisation-based weight allocation.

The temporal separation of flow parameter optimisation and weight learning prevents the instability commonly associated with joint optimisation of heterogeneous architectures, particularly when combining parametric and non-parametric approaches with fundamentally different convergence characteristics. This sequential approach, combined with performance-based weight allocation through a softmax-parameterised gating function, enables the emergence of natural specialisation patterns where each component assumes responsibility for modelling the distributional aspect where it demonstrates superior performance.

The resulting framework effectively implements a form of Bayesian model averaging, where the mixture automatically selects the most appropriate architectural prior for different regions of the latent space. Through this adaptive combination of complementary inductive biases, autoregressive assumptions, coupling layer constraints, and iterative Gaussianization-AMF-VI, the algorithm achieves a robust posterior approximation that transcends the limitations of individual flow architectures while maintaining computational tractability and numerical stability throughout the training process.

3 Datasets and Evaluation Protocol

We evaluate six canonical 2D posterior families that span smooth, non-convex, and highly multimodal geometries: *Banana* (warped Gaussian with curved level sets), *X-shape* (crossing modes with anisotropic covariance), *Bimodal* (two well-separated modes), *Multimodal* (five-component mixture), *Two-moons* (nonlinear manifold support), and *Rings* (concentric annuli). Each family is instantiated by a fixed data generator; the same generator is used for all methods. We provide three example visualisations in the first column of Fig. 2. For each dataset, we draw independent training and evaluation samples from the generator and report metrics on held-out evaluation

samples. Unless otherwise stated, we report the mean performance over repeated runs (with different random seeds) and use a single representative seed for qualitative figures. All baselines use their standard training losses and architectures; hyper-parameters (epochs, batch size, learning rate) are kept constant across datasets to isolate shape effects.

We report the *effective number of experts* $N_{\text{eff}} = \exp(H(w))$ computed from the learned global weights to quantify specialisation in Fig. 1. We assess complementary aspects of fit using NLL, $\text{KL}(p\|q)$, Wasserstein-2 (W_2), and MMD (unbiased/biased). Table 1 summarises definitions and motivation behind the choice of these metrics.

Table 1: Metrics, expressions, and rationale. * “u” = unbiased U-statistic; “b” = biased V-statistic (lower variance).

Metric	Expression	Why use here
NLL	$-\mathbb{E}_{z \sim p} [\log q(z)] = H(p) + \text{KL}(p\ q)$	Proxy for the VI objective; penalises mode dropping (via $\text{KL}(p\ q)$).
$\text{KL}(p\ q)$	$\mathbb{E}_{z \sim p} \left[\log \frac{p(z)}{q(z)} \right]$	Mass-covering divergence aligned with ELBO optimisation.
W_2	$\left(\inf_{\gamma \in \Pi(p, q)} \mathbb{E}_{(x, y) \sim \gamma} \ x - y\ _2^2 \right)^{1/2}$	Transport/geometry aware; captures shape and displacement.
MMD (u/b)*	$\text{MMD}_k^2(p, q) = \mathbb{E}_{p, p} k + \mathbb{E}_{q, q} k - 2 \mathbb{E}_{p, q} k$	Nonparametric two-sample discrepancy complementary to NLL/KL/OT.

4 Experimental Analysis

In this section, we assess the robustness and consistency of **AMF-VI** by comparing it against single-flow baselines, across six canonical posterior families which span unimodal, curved, and multimodal geometries to stress-test shape robustness. Performance is reported under five complementary metrics, and complete results are summarised in 2.

We organise the quantitative analysis into three parts: (i) *overall likelihood*, assessed by NLL; (ii) *transport behaviour*, via Wasserstein-2; and (iii) *divergences/discrepancies*, using $\text{KL}(p\|q)$ and MMD, to expose complementary facets of performance across datasets.

Overall likelihood. Across six qualitatively different posterior families, **AMF-VI** attains the lowest negative log-likelihood (NLL) on *every* dataset in Table 2: 3.463 (*banana*), 3.295 (*X-shaped*), 3.154 (*bimodal*), 3.429 (*five-mode*), 1.188 (*two-moons*), and 2.585 (*rings*). In contrast, single-flow baselines fluctuate with geometry: MAF diverges on *banana*, *bimodal* and *five-mode* ($\text{NLL} = \infty$), REALNVP lags on *two-moons* and *rings* (2.343 and 3.349), and RBIG trails on *banana* (4.131). Because NLL directly reflects the variational objective, these results support the claim of *shape-robust* inference with a single configuration, while highlighting the brittleness of individual flow families across heterogeneous posteriors (Dinh et al., 2016; Papamakarios et al., 2017).

Transport behaviour. On Wasserstein-2 distance, **AMF-VI** is best on *X-shaped* (0.254 vs. 0.286/0.364/0.302), the *five-mode* mixture (0.218 vs. 0.231/0.226/0.267) and *two-moons* (0.107 vs. 0.116/0.114/0.122), and *near-best* on *bimodal* (0.174, second to RBIG at 0.169). Specialised baselines occasionally win on specific geometries, MAF on *banana* and *five-mode*; RBIG on *rings* and *bimodal*, but **AMF-VI** avoids the sharp regressions seen elsewhere and typically ranks first or second, with *banana* being the main exception (third). This aligns with known inductive biases: coupling flows and Gaussianization can excel in niches yet underperform on other shapes (Dinh et al., 2016; Laparra et al., 2011; Villani, 2008).

Divergences and discrepancies. KL and MMD trends corroborate the likelihood picture. **AMF-VI** achieves the lowest $\text{KL}(p\|q)$ on four out of six data sets with *X-shaped* (0.037), *bimodal* (0.024), and *five-mode* (0.029), and ties REALNVP on *rings* (0.042); it is close but not best on *two-moons* (0.018 vs. MAF’s 0.014) and *banana* (0.047 vs. MAF’s 0.035). For MMD, **AMF-VI** is best on *bimodal* (u/b: 0.004/0.026), *five-mode* (0.015/0.032), and *two-moons* (0.003/0.017), and second on *X-shaped* (0.031/0.042), *five-mode* (0.023/0.037) and *rings* (0.037/0.046); *banana* remains a favourable case for MAF. Taken together with uniformly superior NLL, these findings indicate that a heterogeneous mixture adapts component usage to target geometry, delivering

reliable performance across shape regimes while single-flow baselines oscillate between strong and weak modes (or fail outright) (Papamakarios et al., 2017; Laparra et al., 2011).

Table 2: Quantitative results on six posterior families. **Bold** and underlined values denote best and second best, respectively.

Dataset	Metric	AMF-VI	REALNVP	MAF	RBIG
Banana	NLL	3.463	<u>4.026</u>	∞	4.131
	KL	0.047	<u>0.044</u>	0.035	0.066
	W2	0.267	<u>0.251</u>	0.222	0.308
	MDD-u	0.031	<u>0.026</u>	0.018	0.039
	MDD-b	0.042	<u>0.038</u>	0.034	0.048
X-shaped	NLL	3.295	4.048	4.795	4.049
	KL	0.037	<u>0.040</u>	0.044	0.077
	W2	0.254	<u>0.286</u>	0.364	0.302
	MDD-u	<u>0.031</u>	0.024	0.036	0.049
	MDD-b	0.042	0.037	0.046	0.056
Bimodal	NLL	3.154	3.839	∞	<u>3.589</u>
	KL	0.024	0.036	0.035	<u>0.025</u>
	W2	<u>0.174</u>	0.195	0.199	0.169
	MDD-u	0.004	0.010	0.014	<u>0.009</u>
	MDD-b	0.026	<u>0.028</u>	0.031	0.029
Multimodal	NLL	3.429	<u>3.852</u>	∞	4.096
	KL	0.029	<u>0.037</u>	0.038	0.050
	Wasserstein	0.218	0.231	<u>0.226</u>	0.267
	MDD-un	0.023	<u>0.025</u>	0.029	0.044
	MDD-biased	0.037	<u>0.038</u>	0.040	0.052
Two-moons	NLL	1.188	2.343	<u>1.661</u>	1.741
	KL	0.018	0.020	0.014	0.049
	W2	0.104	0.116	<u>0.110</u>	0.124
	MDD-u	0.000	0.011	<u>0.005</u>	0.011
	MDD-b	0.017	0.027	<u>0.021</u>	0.026
Rings	NLL	2.585	3.349	3.549	<u>3.263</u>
	KL	0.042	0.042	0.088	<u>0.063</u>
	W2	<u>0.354</u>	0.427	0.519	0.295
	MDD-u	<u>0.037</u>	0.057	0.085	0.008
	MDD-b	<u>0.046</u>	0.064	0.090	0.030

Figure 1 visualises the learned mixture weights for REALNVP, MAF, and RBIG across the six posterior families, showing adaptation to geometry rather than collapse to a single expert. For *Banana*, the gate assigns almost zero weight to MAF (0.010) and splits mass between REALNVP (0.505) and RBIG (0.484), consistent with MAF’s divergence on this dataset and the stronger baselines among the other two. On *X-shaped*, REALNVP and RBIG receive comparable weight (0.403/0.406), aligning with the strong transport/discrepancy performance of these families, while *AMF-VI* still achieves the best NLL/KL in Table 2. On the *Bimodal* target, RBIG is emphasised (0.515), matching its favourable W_2 score (with *AMF-VI* second), whereas *AMF-VI* remains best on NLL/MMD. For the *Multimodal* (five-mode) case, the gate prioritises REALNVP (0.517) and RBIG (0.427) and downweights MAF (0.056), reflecting MAF’s unstable likelihood there despite its narrow advantage on W_2 ; the mixture consequently attains the best NLL/KL and MMD. On *Two-moons*, REALNVP and MAF receive similar weights (0.376/0.348) while RBIG is down-weighted (0.276), matching the stronger transport/divergence behaviour of the former pair and the best NLL/ W_2 of *AMF-VI*. Finally, for *Rings* the allocation is broadly balanced (0.362/0.295/0.343), consistent with the absence of a single dominant baseline across metrics (with RBIG leading W_2 /MMD and *AMF-VI* leading NLL). Overall, the weights remain distributed and adjust to target geometry, indicating that the mixture exploits complementary inductive biases without component collapse, which helps explain the stable, across-family NLL gains in Table 2.

To quantify how many experts are effectively used by the gate, we report $N_{\text{eff}}(w) = \exp(H(w))$, where H is the Shannon entropy of the *global* mixture weights ($N_{\text{eff}} \in [1, K]$, here $K=3$; 1 indicates collapse, 3 a perfectly balanced mix). Across datasets, we obtain: *Banana* 2.10, *X-shaped* 2.86, *Bimodal* 2.52, *Multimodal* 2.38, *Two-moons* 2.98, and *Rings* 2.99 (mean ≈ 2.64 , range [2.10, 2.99]). These values confirm *no component collapse* and *controlled specialization*: near-three on *Two-moons/Rings* indicates broad participation of all experts, whereas a lower value on *Banana* reflects the two-expert allocation observed in Figure 1. Overall, N_{eff} trends agree with the weight profiles and help explain the robust, across-family NLL gains.

Figure 2 presents qualitative samples for three representative posterior families, (TOP) *X-shaped*, (MIDDLE)

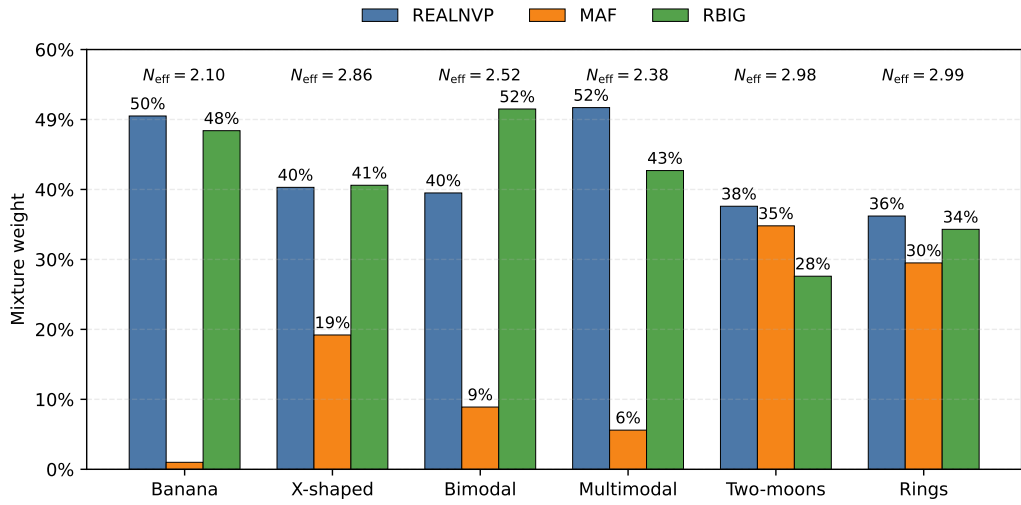


Figure 1: Learned mixture weights per dataset for *AMF-VI* across the three flow components (REALNVP, MAF, RBIG).

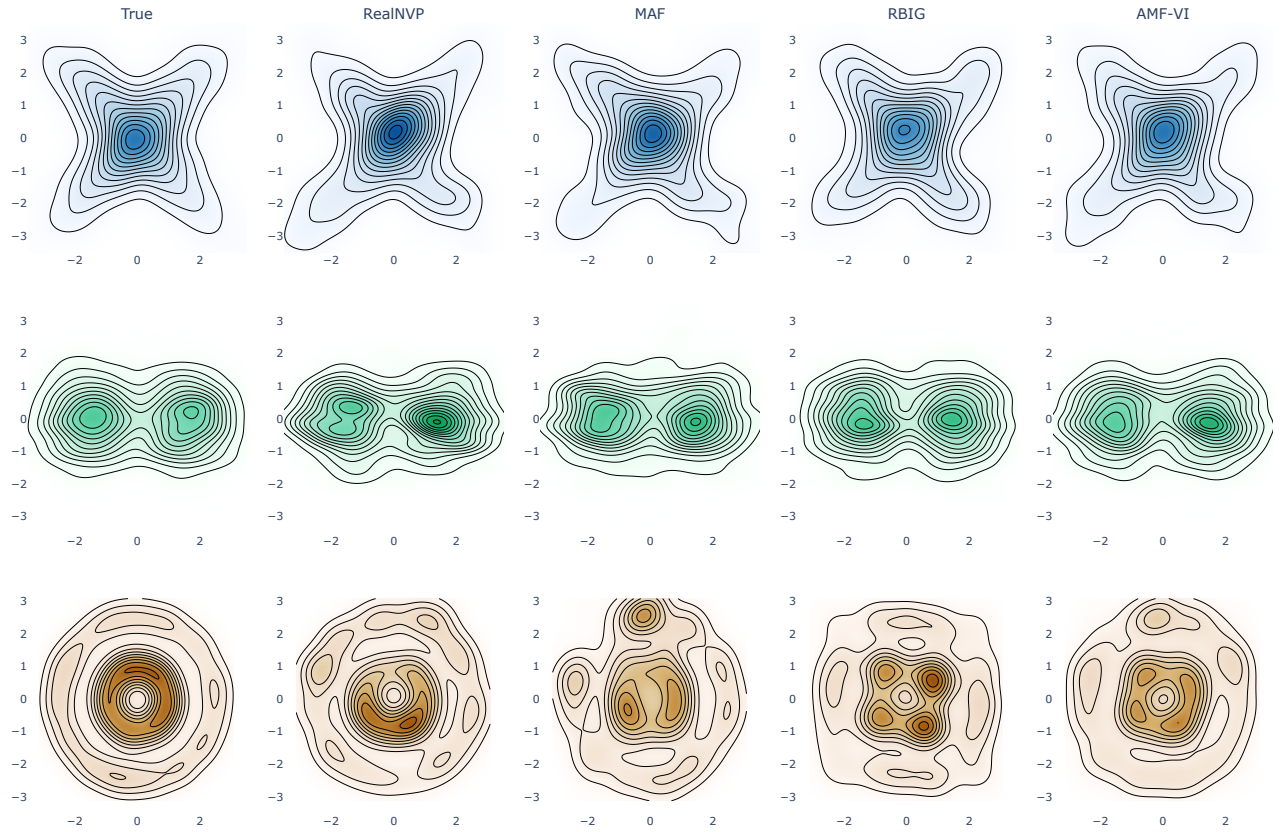


Figure 2: Qualitative comparison on three posterior families, (TOP) *X-shaped*, (MIDDLE) *Bimodal*, and (BOTTOM) *Rings*. Each subfigure shows (left→right) true data and samples from REALNVP, MAF, RBIG, and **AMF-VI**.

Bimodal, and (BOTTOM) *Rings*, contrasting our *AMF-VI* against single-flow baselines (REALNVP, MAF, RBIG). We read these visuals in conjunction with the quantitative results in Table 2. Evaluating Figure 2-(TOP), *AMF-VI* reconstructs the four arms with clean angular structure and limited spurious mass near the

centre, while REALNVP captures the cross but is more diffuse at the tips; MAF visibly blurs the arms and RBIG concentrates too much mass centrally. This matches Table 2: *AMF-VI has the best NLL* (3.295) and *best W_2* (0.254), whereas REALNVP achieves slightly lower MDD values (MDD-u 0.024, MDD-b 0.037) at the cost of worse NLL (4.048).

Figure 2-(MIDDLE), *AMF-VI* clearly resolves the two separated modes with minimal bridging mass; REALNVP produces broader lobes, MAF shows mode-bridging, and RBIG remains comparatively diffuse. Quantitatively, *AMF-VI leads on NLL* (3.154), *KL* (0.024), and *both* MDDs (MDD-u 0.004, MDD-b 0.026), and is *second-best* on W_2 (0.174), slightly behind RBIG (0.169). This indicates high fidelity at data locations together with strong global geometry. Lastly, Figure 2-(BOTTOM), *AMF-VI* reconstructs both rings with mild angular irregularities; REALNVP forms rings but with azimuthal drift; MAF exhibits spoke-like artefacts; RBIG appears “square-ish.” Despite that visual artifact, RBIG scores best on *radial*-dominated metrics (W_2 0.295; MDD-u 0.008; MDD-b 0.030), while *AMF-VI achieves the best NLL* (2.585) and ties REALNVP on *KL* (0.042). This pattern reflects that transport and RBF-MMD emphasise radial alignment of the two rings, whereas NLL is more sensitive to local density at true data locations.

5 Conclusion

We introduced *AMF-VI*, a heterogeneous mixture of normalising flows trained by sequentially fitting expert flows (Stage 1) followed by *post-hoc* likelihood-driven estimation of *global* mixture weights (Stage 2). Across six canonical posterior families, banana, X-shape, two-moons, rings, a bimodal, and a five-mode mixture, *AMF-VI* achieves the *lowest* NLL on all datasets and remains competitive on transport/discrepancy metrics (Table 2). The learned weights are interpretable and non-collapsed (e.g., $N_{\text{eff}} \in [2.10, 2.99]$, mean ≈ 2.64), indicating controlled specialisation rather than single-expert dominance. Qualitatively, the gate emphasises experts whose inductive biases align with geometry (e.g., REALNVP/RBIG on *banana*; more balanced REALNVP/MAF on *two-moons*), which helps explain stable performance even when a baseline fails (e.g., MAF divergence on *banana/bimodal* does not propagate to the mixture).

Compute/memory scale roughly linearly with the number of experts K ; for narrowly scoped posteriors, a single deeper flow might be cheaper. Our Stage 2 uses *global* (data-agnostic) weights rather than per-sample gating and can be sensitive to noisy likelihood estimates if weights become overly peaked (we mitigate with smoothing/floors). Experiments focus on low-to-moderate dimensional targets and canonical shapes; scaling to high-dimensional, constrained, or strongly multi-modal scientific posteriors (and amortised settings) remains open. Performance also depends on the expert set; adding spline/NSF or continuous-time flows could improve coverage at the cost of design complexity.

Promising directions include mixture-aware training (e.g., responsibility-weighted objectives) while retaining the two-stage pipeline, principled specialisation controls (e.g., information-theoretic regularisation or N_{eff} targeting), and extending to amortised inference and higher-dimensional benchmarks. Applying *AMF-VI* to domain-specific posteriors where reliability is critical is a natural next step.

References

Ang, A. and Bekaert, G. (2002). Regime switches in interest rates. *Journal of Business & Economic Statistics*, 20(2):163–182.

Behrmann, J., Grathwohl, W., Chen, R. T., Duvenaud, D., and Jacobsen, J.-H. (2019). Invertible residual networks. In *International conference on machine learning*, pages 573–582. PMLR.

Bengio, Y., Louradour, J., Collobert, R., and Weston, J. (2009). Curriculum learning. In *Proceedings of the 26th annual international conference on machine learning*, pages 41–48.

Berg, R. v. d., Hasenclever, L., Tomczak, J. M., and Welling, M. (2018). Sylvester normalizing flows for variational inference. *arXiv preprint arXiv:1803.05649*.

Bishop, C. M. (2006). *Pattern Recognition and Machine Learning*. Springer.

Bishop, C. M. and Nasrabadi, N. M. (2006). *Pattern recognition and machine learning*, volume 4. Springer.

Blei, D. M., Kucukelbir, A., and McAuliffe, J. D. (2017a). Variational inference: A review for statisticians. *Journal of the American statistical Association*, 112(518):859–877.

Blei, D. M., Kucukelbir, A., and McAuliffe, J. D. (2017b). Variational inference: A review for statisticians. *Journal of the American Statistical Association*, 112(518):859–877.

Breiman, L. (2001). Random forests. *Machine learning*, 45(1):5–32.

Che, T., Li, Y., Jacob, A. P., Bengio, Y., and Li, W. (2016). Mode regularized generative adversarial networks. *arXiv preprint arXiv:1612.02136*.

Chen, R. T., Rubanova, Y., Bettencourt, J., and Duvenaud, D. K. (2018). Neural ordinary differential equations. *Advances in neural information processing systems*, 31.

Dempster, A. P., Laird, N. M., and Rubin, D. B. (1977). Maximum likelihood from incomplete data via the em algorithm. *Journal of the Royal Statistical Society, Series B*, 39(1):1–38.

Dinh, L., Sohl-Dickstein, J., and Bengio, S. (2016). Density estimation using real nvp. *arXiv preprint arXiv:1605.08803*.

Finn, C., Abbeel, P., and Levine, S. (2017). Model-agnostic meta-learning for fast adaptation of deep networks. In *International conference on machine learning*, pages 1126–1135. PMLR.

Hamilton, J. D. (1989). A new approach to the economic analysis of nonstationary time series and the business cycle. *Econometrica: Journal of the econometric society*, pages 357–384.

Izmailov, P., Kirichenko, P., Finzi, M., and Wilson, A. G. (2019). Semi-supervised learning with normalizing flows. *arXiv preprint arXiv:1912.13025*.

Jacobs, R. A., Jordan, M. I., Nowlan, S. J., and Hinton, G. E. (1991). Adaptive mixtures of local experts. *Neural computation*, 3(1):79–87.

Kingma, D. P. and Welling, M. (2013). Auto-encoding variational bayes. *arXiv preprint arXiv:1312.6114*.

Kobyzev, I., Prince, S. J., and Brubaker, M. A. (2020). Normalizing flows: An introduction and review of current methods. *IEEE transactions on pattern analysis and machine intelligence*, 43(11):3964–3979.

Kobyzev, I., Prince, S. J. D., and Brubaker, M. A. (2021). Normalizing flows: An introduction and review of current methods. *IEEE Transactions on Pattern Analysis and Machine Intelligence*, 43(11):3964–3979.

Lakshminarayanan, B., Pritzel, A., and Blundell, C. (2017). Simple and scalable predictive uncertainty estimation using deep ensembles. *Advances in neural information processing systems*, 30.

Laparra, V., Camps-Valls, G., and Malo, J. (2011). Iterative gaussianization: From ica to random rotations. *IEEE Transactions on Neural Networks*, 22(4):537–549.

Loaiza-Ganem, G. and Cunningham, J. P. (2019). The continuous bernoulli: fixing a pervasive error in variational autoencoders. *Advances in Neural Information Processing Systems*, 32.

Makansi, O., Ilg, E., Çiçek, Ö., and Brox, T. (2019). Overcoming limitations of mixture density networks: A sampling and fitting framework for multimodal future prediction. In *CVPR*, pages 7144–7153.

McLachlan, G. J. and Krishnan, T. (2008). *The EM algorithm and extensions*. John Wiley & Sons.

Ng, K. H. and Zammit-Mangion, A. (2024). Mixture modelling using normalising flows for spherical density estimation. *Advances in Data Analysis and Classification*, 18:103–120.

Nichol, A., Achiam, J., and Schulman, J. (2018). On first-order meta-learning algorithms. *arXiv preprint arXiv:1803.02999*.

Papamakarios, G., Nalisnick, E., Rezende, D. J., Mohamed, S., and Lakshminarayanan, B. (2021). Normalizing flows for probabilistic modeling and inference. *Journal of Machine Learning Research*, 22(57):1–64.

Papamakarios, G., Pavlakou, T., and Murray, I. (2017). Masked autoregressive flow for density estimation. In *Advances in Neural Information Processing Systems (NeurIPS)*.

Pires, G. G. P. F. and Figueiredo, M. A. T. (2020). Variational mixture of normalizing flows. In *European Symposium on Artificial Neural Networks (ESANN)*. arXiv:2009.00585.

Rezende, D. and Mohamed, S. (2015). Variational inference with normalizing flows. In *International conference on machine learning*, pages 1530–1538. PMLR.

Shazeer, N., Mirhoseini, A., Maziarz, K., Davis, A., Le, Q., Hinton, G., and Dean, J. (2017). Outrageously large neural networks: The sparsely-gated mixture-of-experts layer. *arXiv preprint arXiv:1701.06538*.

Stimper, V., Schölkopf, B., and Hernández-Lobato, J. M. (2022). Resampling base distributions of normalizing flows. In *Proceedings of Machine Learning Research (AISTATS)*, volume 151, pages 1–22.

Sutton, R. S., Barto, A. G., et al. (1998). *Reinforcement learning: An introduction*, volume 1. MIT press Cambridge.

Tomczak, J. and Welling, M. (2018). Vae with a vampprior. In *International conference on artificial intelligence and statistics*, pages 1214–1223. PMLR.

Villani, C. (2008). *Optimal Transport: Old and New*, volume 338 of *Grundlehren der mathematischen Wissenschaften*. Springer.

Wakefield, J. (2007). Disease mapping and spatial regression with count data. *Biostatistics*, 8(2):158–183.

Wang, D., Liu, H., and Liu, Q. (2018). Variational inference with tail-adaptive f-divergence. In *Advances in Neural Information Processing Systems (NeurIPS)*.